Revista Mexicana de Astronomía y Astrofísica, **43**, 101–121 (2007)

THE PROPERTIES OF OPTICAL FEII EMISSION LINES OF AGN WITH DOUBLE-PEAKED BROAD EMISSION LINES

Xue-Guang Zhang,[1,2] Deborah Dultzin-Hacyan,[1] and Ting-Gui Wang[2]

Received 2006 May 24; accepted 2006 October 17

RESUMEN

Estudiamos las propiedades de una muestra de 27 núcleos activos de galaxias (NAGs) con perfil de doble pico (dbp) en las líneas anchas de emisión de baja ionización, tomados del DR4. Nuestro primer resultado es que todo el espectro de emisión en el intervalo de 4100 Å a 5800 Å se puede ajustar muy bien mediante un modelo de emisión en un disco de acreción elíptico. Los mejores ajustes indican que la emisión óptica de las líneas de FeII en los emisores dbp se originan en la misma región del disco que las líneas de Balmer. Encontramos que algunas correlaciones conocidas para los NAGs normales se cumplen también para los dbp. Sin embargo, este resultado debe tomarse con cautela porque el número de objetos es pequeño y porque tenemos un sesgo de selección hacia objetos con emisión de FeII intensa. Mostramos que para los dbp, la masa del agujero negro central parece tener mayor influencia en las propiedades de la emisión de FeII que la tasa de acreción.

ABSTRACT

We study the FeII properties of double-peaked broad low-ionization emission line AGN (dbp emitters) using a sample of 27 dbp emitters from SDSS (DR4). Our first result is that the line spectra in the wavelength range from 4100 Å to 5800 Å can be best fitted by an elliptical accretion disk model.The best fitted results indicate that the optical FeII emission lines of dbp emitters originate from the same region in the accretion disk where the double-peaked Balmer emission lines originate. Some correlations between FeII emission lines and the other broad emission lines for normal AGN can be confirmed for dbp emitters. However, these results should be taken with caution due to the small number of objects and the bias in selecting strong FeII emitters. We show that for dbp emitters, BH masses seems to have more influence on FeII properties than dimensionless accretion rate.

Key Words: **ACCRETION, ACCRETION DISKS — GALAXIES: ACTIVE — QUASARS: EMISSION LINES**

1. INTRODUCTION

The optical FeII emission lines are one of the most important properties of some active galactic nuclei (AGN). Because of the large amounts of FeII emission lines (half-filled 3d-shell leads to thousands of transitions for FeII emission lines) (Moore & Merill 1968; Netzer 1988; Wills et al. 1980; Wills, Netzer, & Wills 1980), it is difficult to clarify many properties of these lines, such as their loci of emission, the mechanism of their excitation, the correlation between FeII lines and other emission lines. The bright object I Zw I (PG 0050+124) has very strong FeII emission lines which can be accurately measured. And thus it has been used to build FeII templates for the subtraction of these lines when reducing quasar spectra in order to properly fit the continuum (Philips 1978; Oke & Lauer 1979; Boroson & Green 1992; Laor et al. 1997; Marziani et al. 2003a).

A detailed study of line-related correlations between FeII and other properties of AGN can be found in Sulentic, Marziani, & Dultzin-Hacyan (2000): there is an outstanding strong anticorrelation between EW(FeII4570)/EW(Hβ) and FWHM($H\beta$) in the context of the so called Eigenvector 1 (E1) pa-

[1]Instituto de Astronomía, Universidad Nacional Autónoma de México, Mexico.

[2]Center for Astrophysics, University of Science and Technology of China, Hefei, Anhui, P.R. China.

rameter space. These authors have defined a population A, FWHM(Hβ_{broad})< 4000 km $\cdot$ s^{-1}, and population B, FWHM(Hβ_{broad})> 4000 km $\cdot$ s^{-1}, which is a cleaner distinction for AGN with strong and weak FeII emission lines than radio loud objects vs. radio quiet objects. A preliminary definition of Eigenvector 1 can be found in Boroson & Green (1992). An updated and more complete version of it includes the interpretation of the observed trends in this parameter space in the context of their physical drivers: BH masses and accretion rate (Sulentic et al. 2006).

There are two main kinds of models which can reproduce the observed shape and equivalent width of FeII emission lines: Photoionization models with microturbulence (Korista et al. 1997; Bottorff et al. 2000; Netzer 1985; Baldwin et al. 2004) in the context of the so called LOC model (Baldwin et al. 1995) and collisionally excited models (Grandi 1981, 1982; Kwan et al. 1995; Dumant, Collin-Souffrin, & Nazaiova 1998; Baldwin et al. 2004). A simple photoionization scheme is not adequate to reproduce the observed FeII lines (Bergeron & Kunth 1980; Collin-Souffrin et al. 1986; Joly 1987; Collin-Souffrin, Hameury & Joly 1988) because of the enhanced FeII emission due to the needed high density ($> 10^{11}$ cm^{-3}) of the emitting clouds (Ferland & Person 1989). Thus, the accretion disk and/or the region near the center produced by shocks along the radio jet provide a natural high density environment for FeII emission lines. Sigut & Pradhan (2003) have examined this assumption for the typical physical conditions of AGN. In their paper, the following excitation mechanisms for FeII emission lines have been considered: continuum fluorescence (Phillips 1978, 1979), collisional excitation (Joly 1991), self-fluorescence among the FeII transitions and fluorescent excitation by Lyα and Lyβ (Penston 1988; Sigut & Pradhan 1998; Verner et al. 1999).

The most commonly accepted outcome from the study of FeII emission lines is that the line width of these lines is the same as that of the other broad low-ionization emission lines such as Hβ, except for several special objects such as HE 1249-0648 and HE 1258-0823 (FWHM($H\beta$) $\gg$ FWHM(FeII)) (Marziani et al. 2003a, 2003b). The best way to determine where the FeII emission lines originate, wheter in the accretion disk or at the base of the jet, is to study the properties of FeII lines from a special kind of AGN which emit double-peaked broad low-ionization Balmer emission lines (dbp emitters). These double-peaked broad lines are believed to originate in the accretion disk near the central Black Hole (BH) (Storchi-Bergmann et al. 2003; Storchi-Bergmann et al. 1997; Storchi-Bergmann et al. 1995; Eracleous et al. 1997; Storchi-Bergmann, Baldwin, & Wilson 1993; Chen & Halpern 1989a; Chen, Halpern, & Filippenko 1989b, Chen, Halpern, & Titarchuk 1997; Halpern et al. 1996; Antonucci, Hurt, & Agol 1996; Sulentic et al. 1990; Shapovalova et al. 2001; Gilbert et al. 1999; Hartnoll & Blackman 2002; Karas, Martocchia, & Subr 2001). Other models have been considered to interpret the origin of double-peaked broad lines, such as the binary black hole model (Begelman, Blandford, & Rees 1980; Gaskell 1983) and the bipolar outflow model (Zheng, Sulentic, & Binette 1990), but they have proved unsuccessful to explain most dbp emitters.

In a previous paper we reported a flat-spectrum radio quiet quasar, SDSS J2125-0813, which has a broad double-peaked Hβ (FWHM($H\beta$) $\sim$15000 km$\cdot s^{-1}$), and strong FeII emission lines at optical bands that have exactly the same line profile as that of the broaddouble-peaked Hβ line (Zhang, Dultzin-Hacyan, & Wang 2006a, hereafter Paper I). In this paper, we select a whole sample of AGN with both double-peaked broad Balmer lines and strong optical FeII emission lines to study the FeII properties of dbp emitters. There are two famous samples of dbp emitters. One consists of 23 objects which are nearly all LINERs from radio galaxies (Eracleous & Halpern 1994, 2003; Eracleous et al. 1995), and the other is made up of 112 objects of which 12% are classified as LINERs (Strateva et al. 2003) selected from SDSS DR2 (York et al. 2000). Recently, we have built a larger sample of dbp emitters from SDSS DR4 (Zhang, Dultzin-Hacyan, & Wang 2007), which includes more than three hundred dbp emitters. Because of the convenience to get the spectra of SDSS, we select dbp emitters with apparent FeII emission lines from the two samples in SDSS (Strateva et al. 2003; Zhang et al. 2007). In Section 2 we list the data of our sample. Section 3 presents the results and then the discussion and conclusions follow in Section 4. The cosmological parameters H_0=75 km s^{-1} Mpc^{-1}, $\Omega_\lambda = 0.7$ and $\Omega_m = 0.3$ have been adopted here.

2. THE SAMPLE

There are 112 dbp emitters selected from SDSS DR2 by Strateva et al. (2003) and more dbp emitters are being selected from SDSS DR4 by Zhang et al. (2007). Because we select dbp emitters from the main catalogs of galaxies and of quasars classified by pipeline of SDSS, with criteria different from those used by Strateva et al. (2003), and because

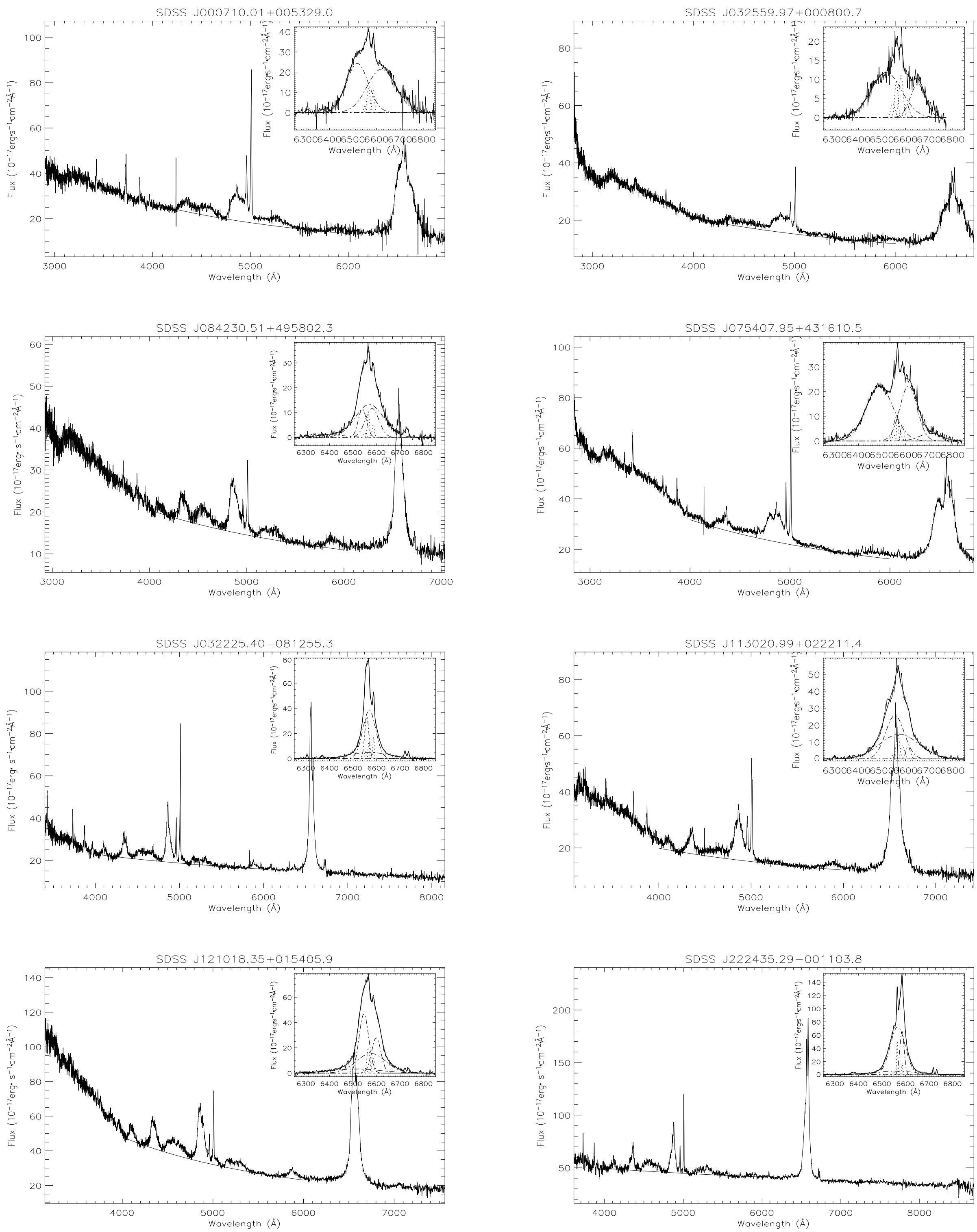

Fig. 1. The spectra of dbp emitters and the continuum under Hβ are shown in the figure. The best fitted results for narrow emission lines near Hα are shown in the upper right panels in each plot. The thin solid line is the spectra after the subtraction of the continuum. The thick solid line represents the best fitted results, the dotted line presents the components for [NII]λ6548,6583Å+$H\alpha_{narrow}$. The dash-dotted line represents the components for broad Hα.

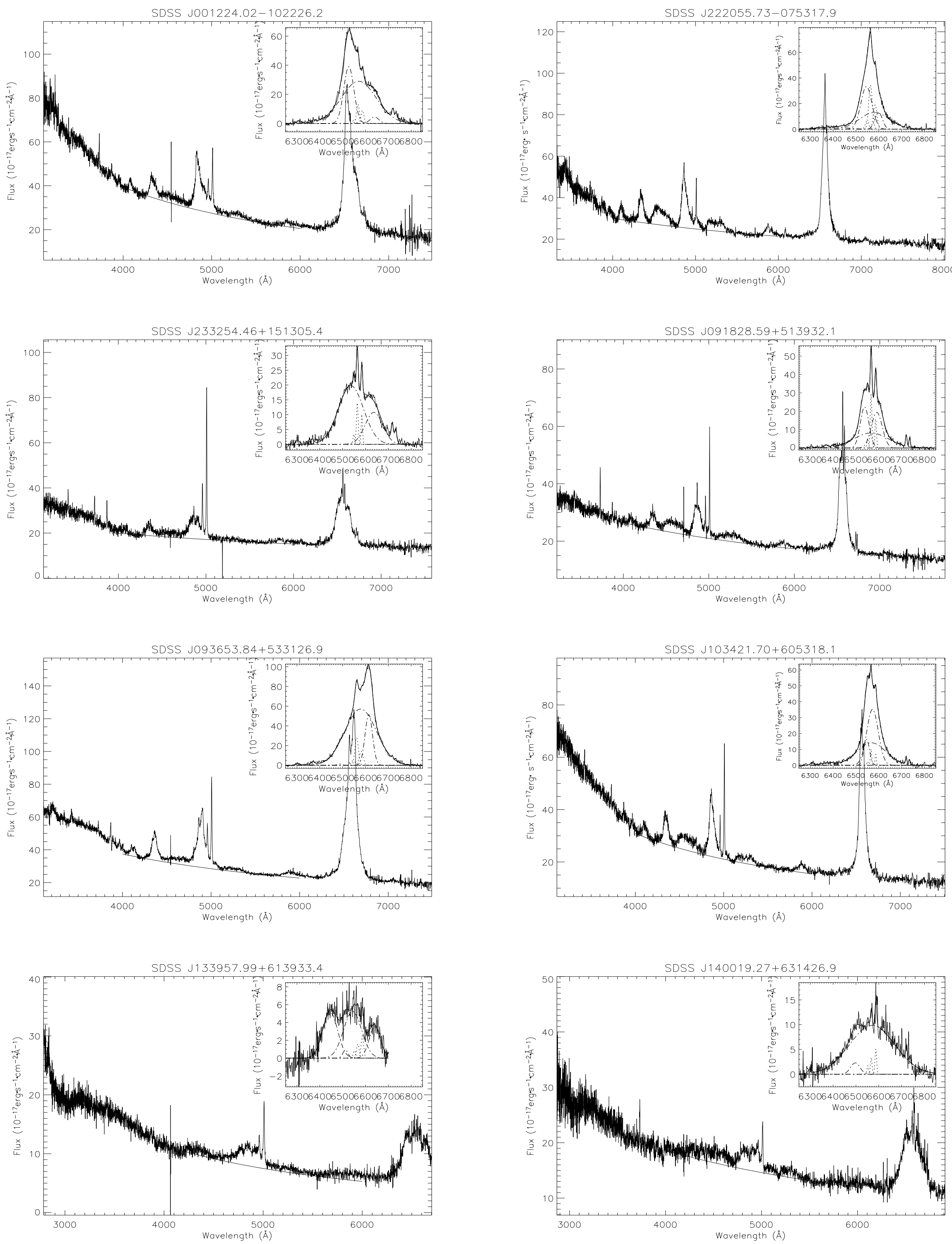

Fig. 1. Continued.

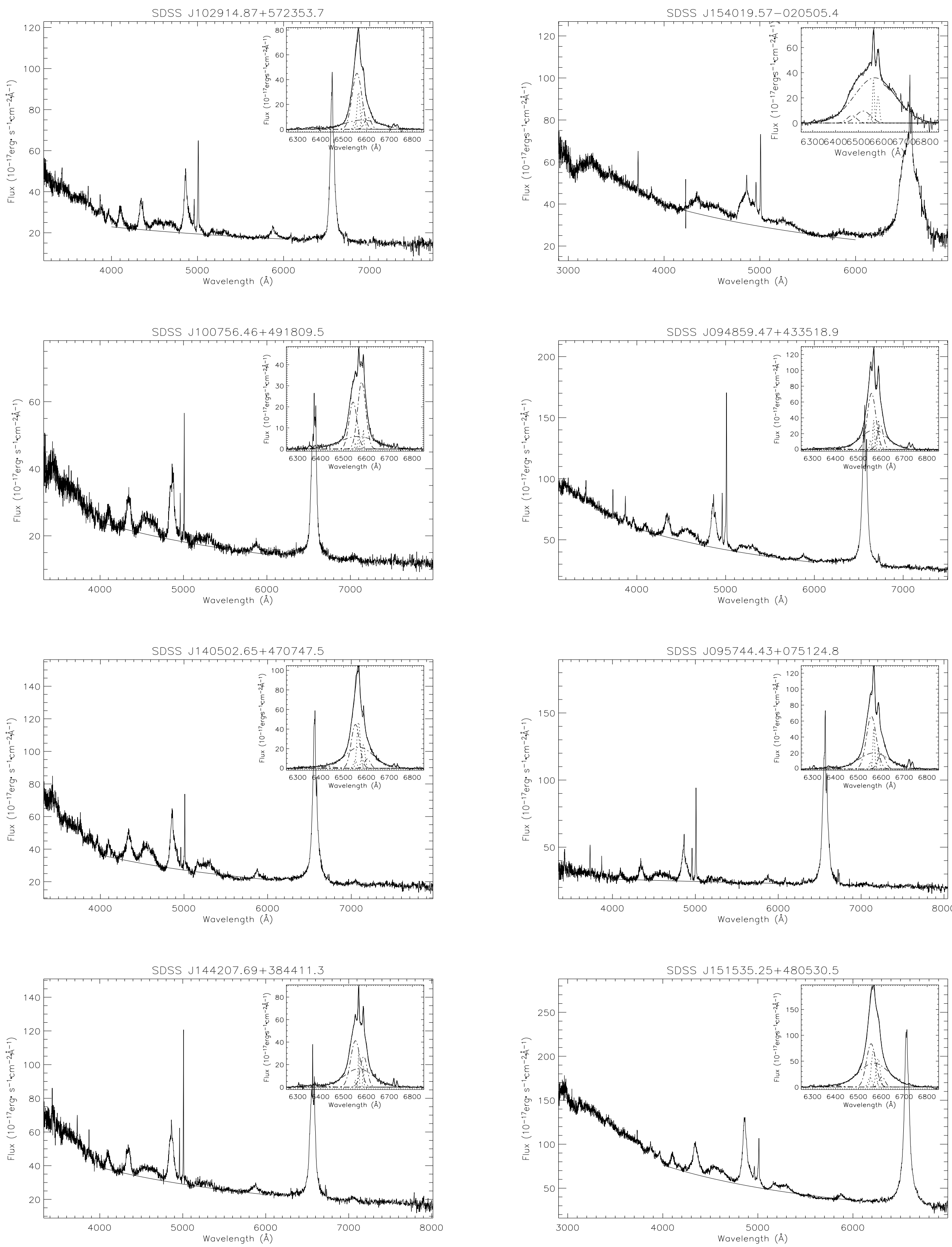

Fig. 1. Continued.

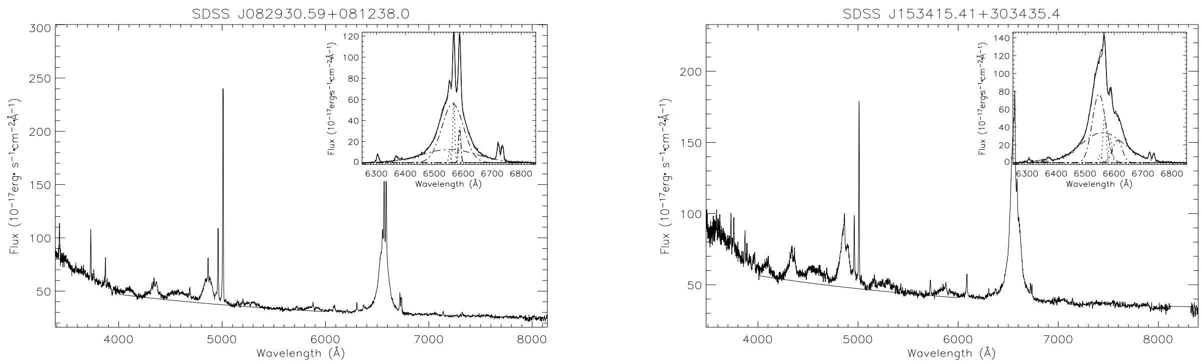

Fig. 1. Continued.

in this paper we simultaneously select dbp emitters with apparent and strong FeII emission lines, even when we use DR4, our sample is smaller (some dbp emitters selected by Strateva et al. (2003) are not included in our sample).

The detailed selection criteria will be described in a forthcoming paper (Zhang et al. 2007). We give here a description of the steps we followed: First, we subtracted the stellar components from the observed spectra by the PCA template method (Hao et al. 2005; Li et al. 2005), if necessary. Then the emission lines, especially Hα+[NII]λ6548, 6583Å, were fitted by Gaussian functions. At least two Gaussian functions, one broad and one narrow, were applied for each permitted emission line, and one Gaussian function for each forbidden emission line. According to the best fitted results obtained by the Levenberg-Marquardt least-squares minimization technique, the AGN with broad emission lines were selected by the following criteria: the line width (σ), and flux of the broad component of Hα should be at least 5 times larger than the measured errors, and also the line width σ of the broad component of Hα should be larger than 800 $\mathrm{km \cdot s^{-1}}$. The value of the summed squared residuals divided by the number of degrees of freedom, χ_1^2, can also be obtained. The value χ_1^2 near to 1 represents whether the parameters of the model are significant for the fit to the emission lines. Because of the complex line profiles of double-peaked emission lines one broad Gaussian function is not the best choice to fit the broad component; the values of χ_1^2 for objects with double-peaked broad Hα should be larger than 1. Thus multi-Gaussian functions (four broad Gaussian functions) are applied for broad emission lines again. Then we obtain the other value of χ_2^2 for each AGN with broad emission lines. For objects with double-peaked broad Hα, the value of χ_2^2 should be much closer to 1. We then select our dbp emitter candidates according to the following criterion: $\chi_1^2 - \chi^2 > 1$, which indicates the observed line profiles cannot be properly fitted by one broad Gaussian function. Finally, we check the dbp emitter candidates one by one by eye, according to whether there are features suggestive of double peaks. We reject the candidates which have asymmetric line profiles of Hα or have multi-Gaussian components with the same center wavelength (where the separation of peaks is less than 10Å).

According to the observed spectra of SDSS, we can easily select the dbp emitters for which the FeII emission lines are evident, especially in the wavelength range from 4100 Å to 5800 Å. Including the object SDSS J2125-0813 we find 27 dbp emitters with apparent FeII emission lines. 12 dbp emitters are selected from the sample of Strateva et al. (2003) and 15 new dbp emitters are selected from SDSS DR4. We show the spectra in Figure 1 (the spectrum of SDSS J2125-0813 can be found in Paper I, here we do not show it again). According to the properties of the spectra, all the 27 dbp emitters are quasars. The other 26 objects have both double-peaked Hα and Hβ emission lines (because we have a limit of less then 0.33 on the redshift of dbp emitters selected from SDSS). As discussed below this allows us a more convenient way to measure and estimate the FeII emission lines. The objects are listed in Table 1.

3. RESULTS

3.1. *Measurement of the line parameters of emission lines*

Due to the presence of double-peaked broad Hα, in order to get the best fitted results for narrow emission lines, there are three to four broad Gaussian functions for the broad components of

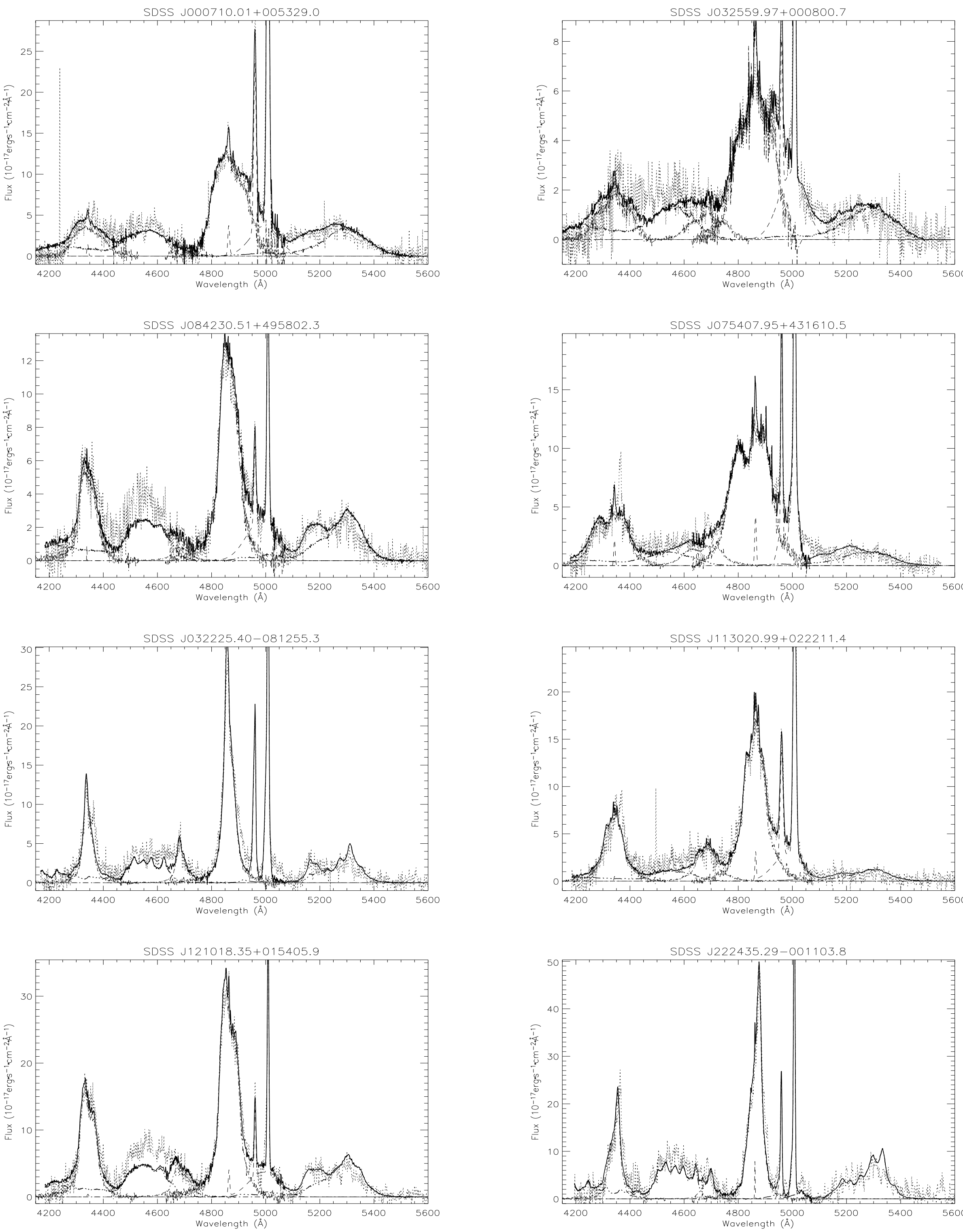

Fig. 2. The best fitted results for the spectra near Hβ of dbp emitters. The dotted line represents the line spectra after the subtraction of the continuum. The thick solid line represents the best fitted results. The dashed line represents the narrow components for [OIII] doublet and/or Hβ and/or Hγ. The dot-dashed line represents the broad components for Hβ, Hγ and/or HeIIλ4686Å. The double dot-dashed line represents the components for FeII emission lines in the wavelength range from 4200 Å to 5600 Å.

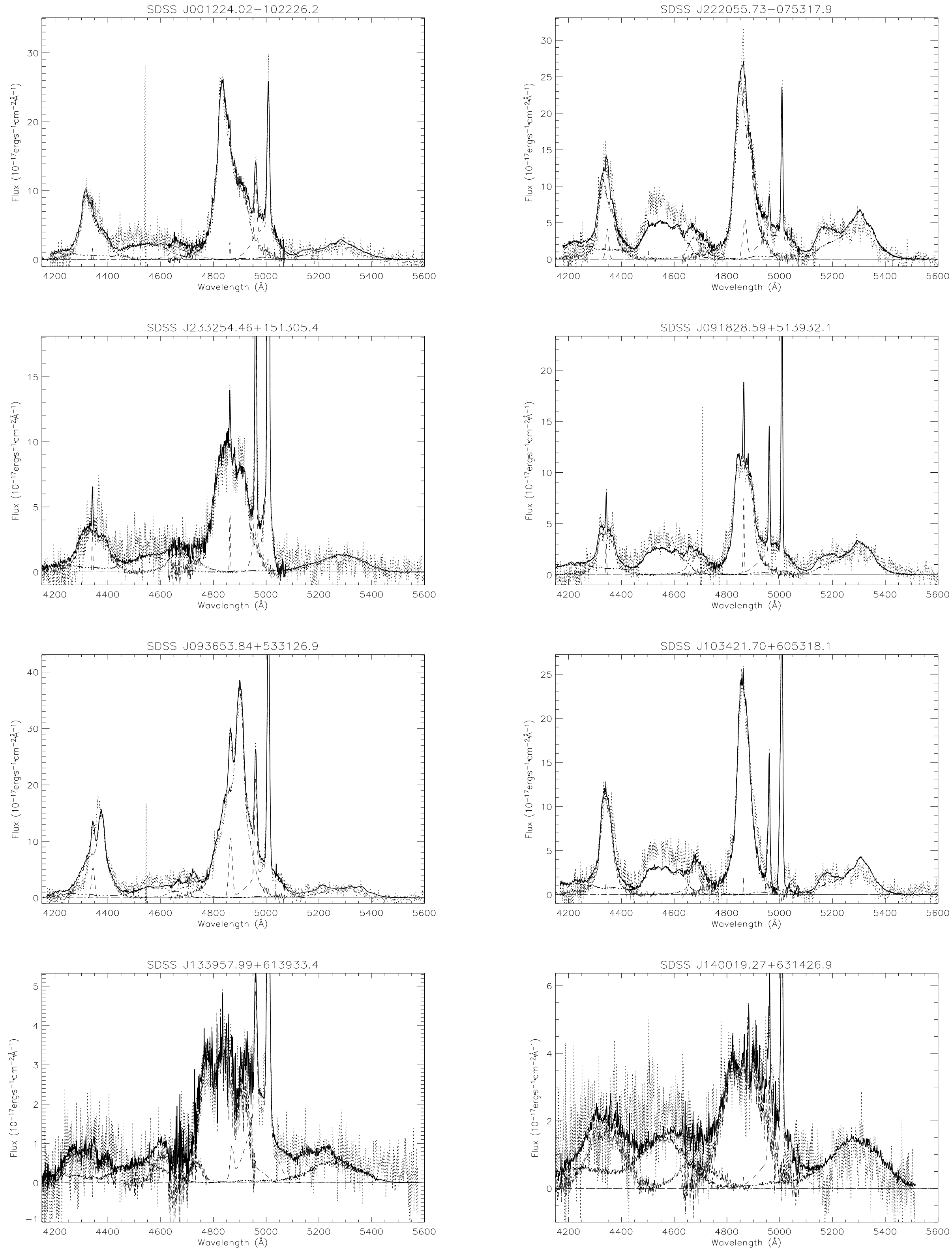

Fig. 2. Continued.

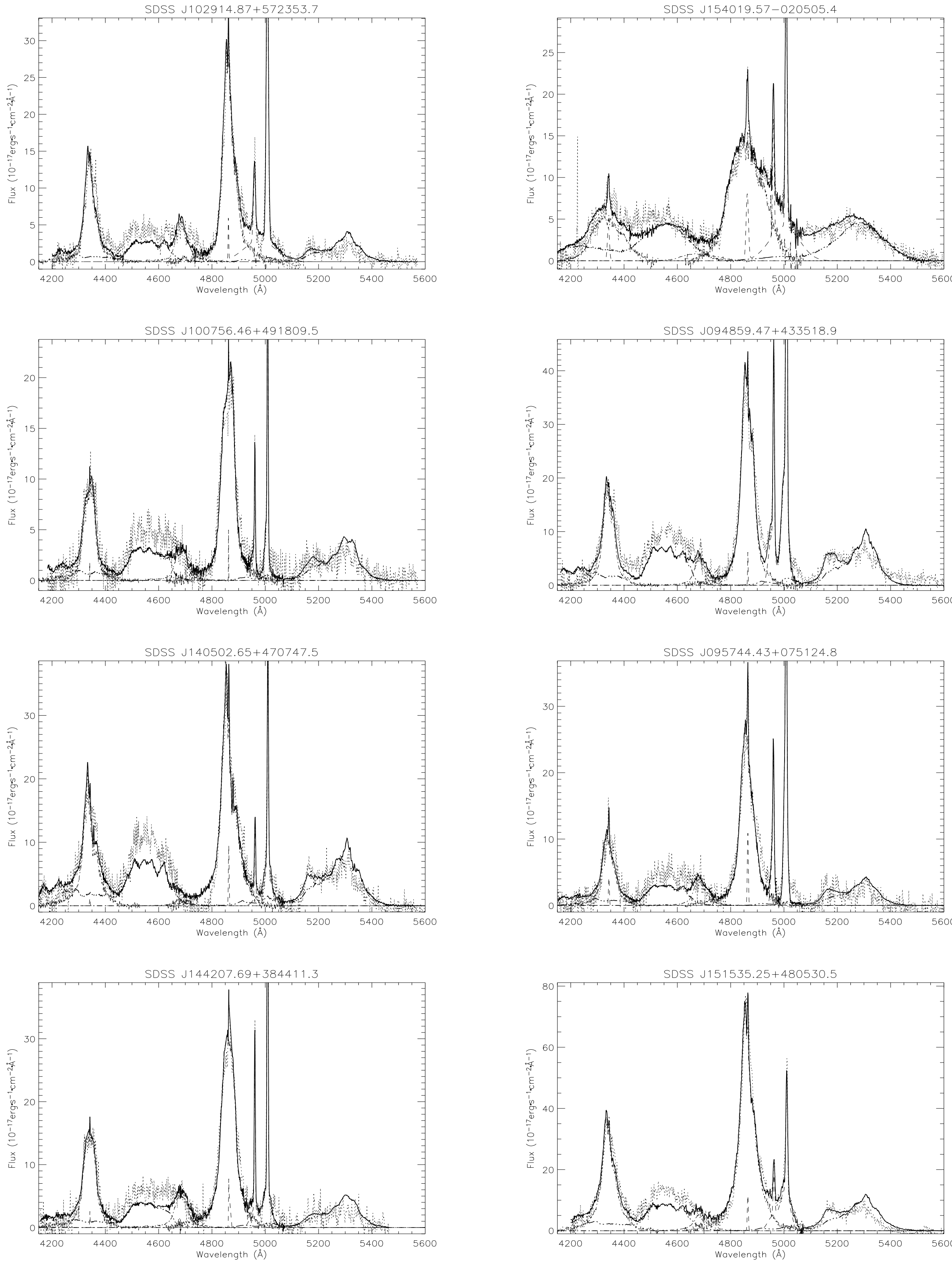

Fig. 2. Continued.

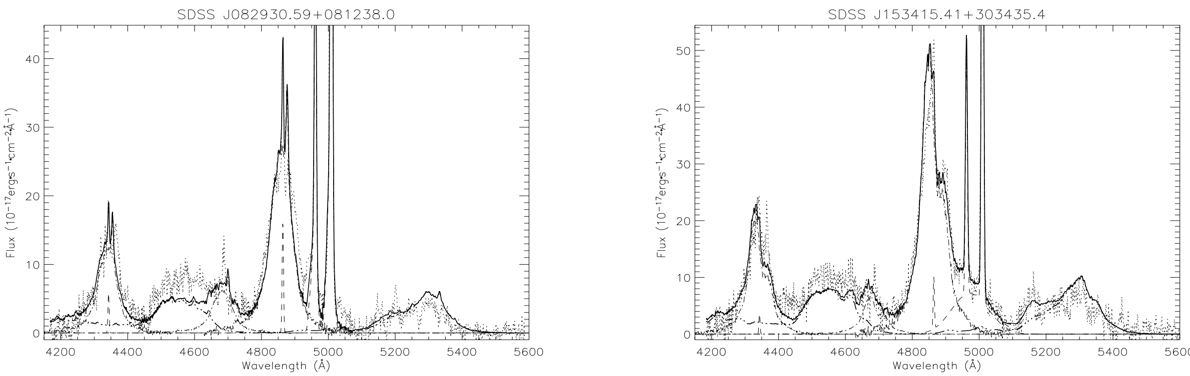

Fig. 2. Continued.

Hα, one single narrow Gaussian function for each narrow emission line in the wavelength range between 6250 Å and 6850 Å and a power law for the continuum. Thus, there are three to four broad Gaussian functions for broad Hα and seven narrow Gaussian functions for [NII]λ6548,6583Å [SII]λ6719,6732Å [OI]λ6300,6363Å and narrow component of Hα. Here, we limit the center wavelength of each doublet to the same redshift, and limit the velocity dispersion of the Gaussian function of each doublet to the same value in velocity space. Furthermore, we fix the flux ratio of [NII]λ6548Å to [NII]λ6583Å to 0.33, limit the line width of narrow emission line (σ_{line}) to be less than 400 $\mathrm{km \cdot s^{-1}}$ and limit the line width of broad emission lines ($\sigma line$) to be larger than 500 $\mathrm{km \cdot s^{-1}}$. The last best fitted results are shown in Figure 1.

According to the best fitted results for narrow emission lines, we can get the broad components of Hα in the wavelength range from 6250 Å and 6850 Å. This provides a better way to measure the FeII emission lines at optical bands and a better way to estimate the model parameters of the accretion disk model. Because of strong FeII emission lines, it is much more difficult to obtain the complete line profile of Hβ. However, we can estimate broad double-peaked Hβ by the line profile of Hα after the subtraction of narrow emission lines. Before proceeding further, we should first subtract the continuum near Hβ. We subtract the continuum according to the best fitted results for the points near 4100 Å and near 5800 Å. The continuum near Hβ is also shown in Figure 1.

Once we obtain the spectra in the wavelength range between 4100 Å and 5800 Å after the subtraction of the continuum, we can fit the spectra as we have done in Paper I, under the assumption that the FeII emission lines come from the same regions as the broad Balmer emission lines:

$$\begin{aligned} f_\lambda &= k_{H\beta} \times H\alpha + k_{H\gamma} \times H\alpha + k_{FeII} \sum FeII \\ &+ k_{FeIII} \sum FeIII + k_{MgI} \sum MgI \\ &+ H\beta_{narrow} + H\gamma_{narrow} + [OIII] \end{aligned} \qquad (1)$$

where k_{line} is the flux ratio of the emission line to broad Hα. The narrow component of Hβ, Hγ and [OIII] doublet can be fitted by narrow Gaussian functions. If necessary, there is a broad component with the same line profile as that of broad Hα for HeIIλ4686Å and two extended Gaussian functions for the extended wings of the [OIII] doublet. The best fitted results are shown in Figure 2. The parameters for the flux ratio of different emission lines are listed in Table 2.

From the fitted results shown in Figure 2 we notice that there are some objects for which the emission lines near Hβ, especially near 4600 Å cannot be adequately fitted. The main reasons are perhaps the following: first, we do not consider the contributions of narrow emission lines of Hγ+[OIII] and CVI emission lines, since they are weak emission lines; second, the lack of accuracy of the continuum subtraction. We fit the continuum under Hβ by a power law function. However, from the study of composite spectra of quasars (Francis et al. 1991; Zheng et al. 1997; Vanden Berk et al. 2001) and especially the study of composite spectra of AGN selected from SDSS, we can see that the continuum should be best fitted by two power laws with a break at $\sim$5000Å. Thus, applying only one power law to fit the continuum under Hβ should lead to some uncertainty.

After the subtraction of narrow emission lines near Hα, we can obtain the parameters of the elliptical accretion disk model (Eracleous et al. 1995) by the Levenberg-Marquardt technique, adjusting the

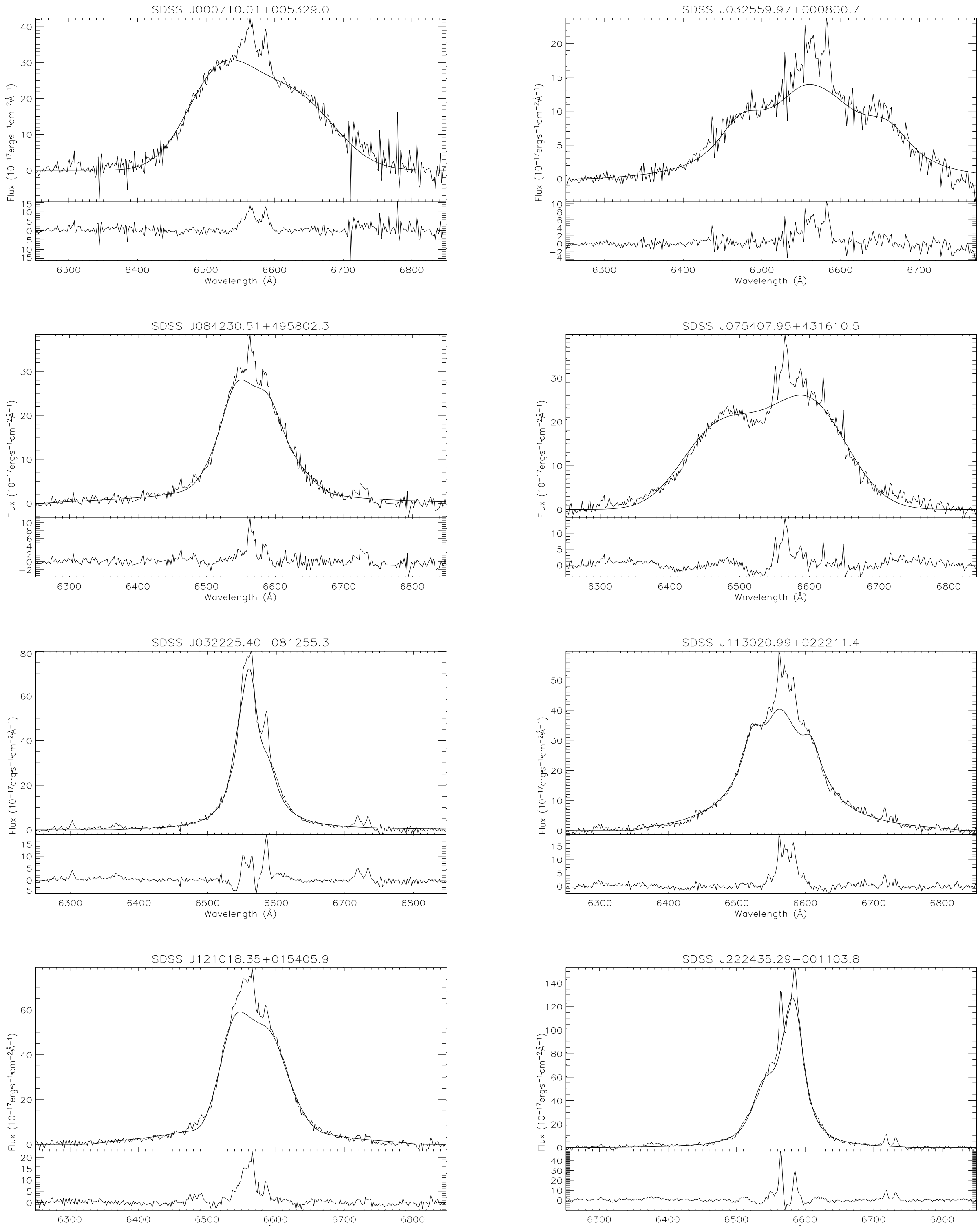

Fig. 3. The best fitted results for double-peaked broad Hα. The lower panel in each plot shows the spectrum after the subtraction of the broad Hα coming from the accretion disk. The model parameters are listed in Table 1.

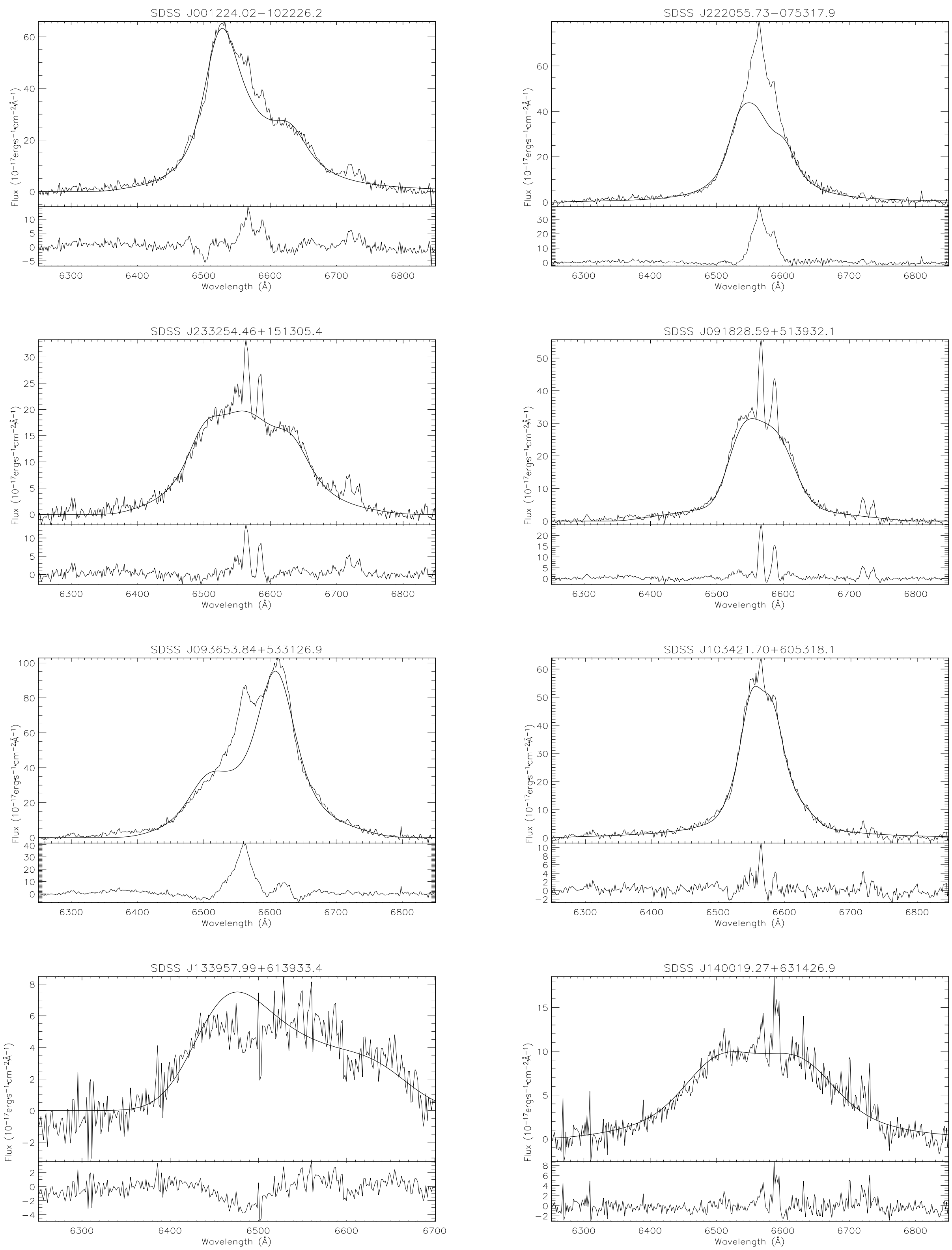

Fig. 3. Continued.

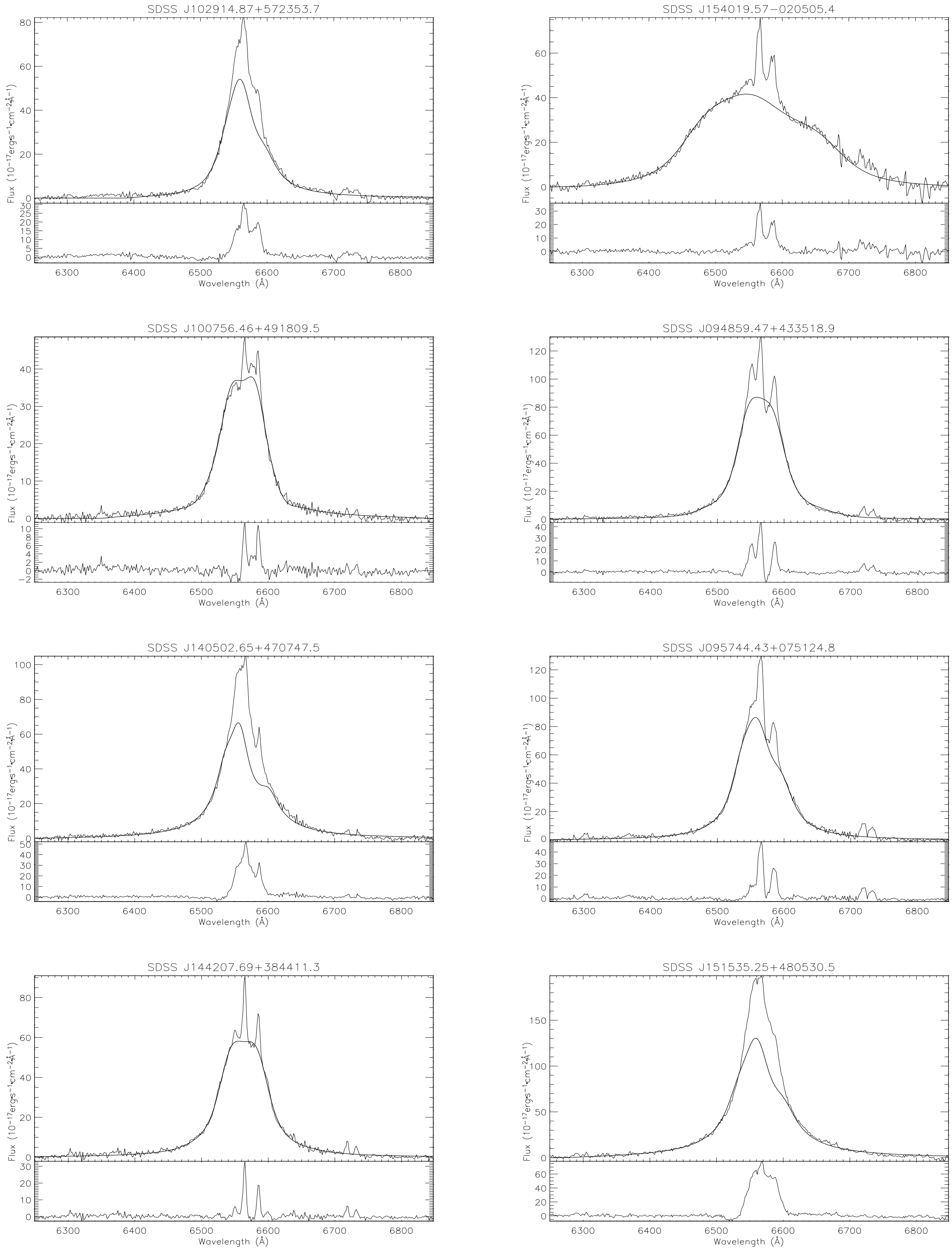

Fig. 3. Continued.

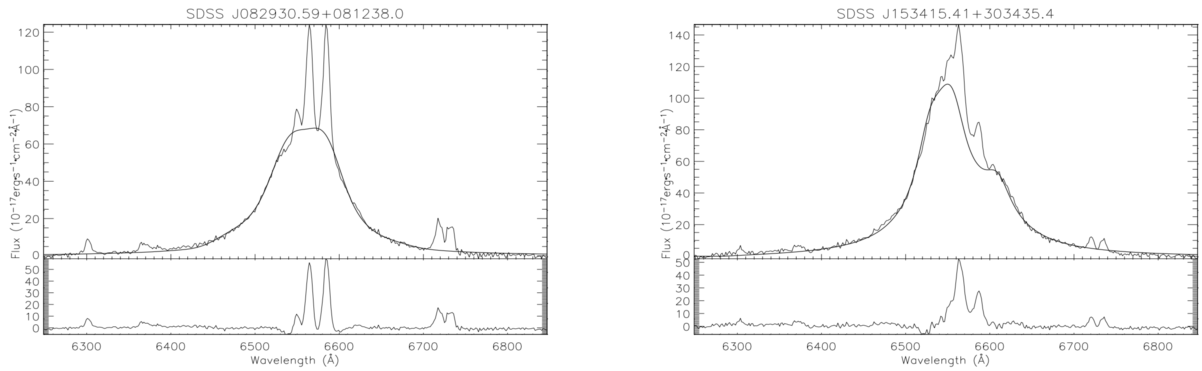

Fig. 3. Continued.

free parameters (MPFIT package in IDL). There are eight free parameters in the elliptical accretion disk model, the inner radius r_{in}, the outer radius r_{out}, the inclination angle of the accretion disk i, the local broadening velocity dispersion σ, the slope of the line emissivity q, the eccentricity e, the orientation angle of the accretion disk ϕ_0 and an amplitude factor k. The best fitted results are shown in Figure 3. The parameters of the accretion disk model for each dbp emitter are listed in Table 2.

We select an elliptical accretion disk model rather than a circular disk plus spiral arm model due to the following considerations. For the elliptical disk model, there are mainly five parameters to determine: the observed line profile, r_{in}, r_{out}, i and e. However, in the circular disk plus spiral arm model, there are another four parameters that dominate the observed line profile. To some extent, we think the uniqueness of the model parameters for an elliptical accretion disk model is better than that of the circular disk plus spiral arm model. Also, we do not select a simple circular accretion disk model because the model cannot be applied for dbp emitters which have a red peak brighter than the blue peak.

Last, we measure the line parameters of broad Hα, such as the line width of Hα, $\sigma_{H\alpha_B}$. The line parameters of the broad component of Hα can be measured by:

$$\lambda_0 = \frac{\int \lambda f_\lambda d\lambda}{\int f_\lambda d\lambda}$$

$$\sigma_g^2 = \frac{\int \lambda^2 f_\lambda d\lambda}{\int f_\lambda d\lambda} - \lambda_0^2 = \frac{\int (\lambda - \lambda_0)^2 f_\lambda d\lambda}{\int f_\lambda d\lambda} .$$

We find that the mean value of f_λ after the subtraction of the continuum is zero for the nearby points on the continuum. However, the mean value $(\lambda - \lambda_0)^2 f_\lambda$ for those points further out is not zero, and becomes larger for the points selected from more extended distances from the center of the emission line, unless we use a smoother background after the subtraction of the continuum for which the value at each point is equal to zero. Thus, we should select cautiously the wavelength to measure the second moment according to the equation above. The wavelength range is selected as follows: after the subtraction of the continuum and the bad pixels, we select the last point for which the flux is equal to the minimum value of the points on the blue side of the emission line (sometimes, the minimum value of the flux is not equal to zero) and select the first point for which the flux is equal to the minimum value of the points on the red side of the emission line. Due to the composite nature of the line profile of double-peaked emission, we think it is more accurate to measure the second moment of the broad Hα using the equation above, than to measure the value of FWHM of Hα according to the standard definition of FWHM, because the flux density of the broad component is the largest one in the composite emission line after the subtraction of the narrow emission lines. The value of $\sigma_{H\alpha_B}$ is listed in Table 1.

3.2. *Properties of FeII emission lines of dbp emitters*

First, we check the correlation between line width of broad Balmer emission lines and strength of FeII emission lines EW(FeII)/EW(Hβ). We show the correlation in Figure 4. The mean value of the second moment of broad Hα is about $3002 \pm 139 \mathrm{km \cdot s^{-1}}$. As pointed out above, we use the second moment of broad Hα rather than FWHM(Hα). The Spearman Rank correlation coefficient is -0.39 with $P_{null} \sim 5\%$. Here, the data include the object SDSS J2125-0813, for which the second moment of broad Hα is estimated from the broad component of Hβ reproduced by the accretion disk model. The

TABLE 1

DATA OF THE SAMPLE

Id	Name	z	m_r	R	$\sigma_{[\mathrm{OIII}]}$ $\mathrm{km \cdot s^{-1}}$	$\sigma_{H\alpha_B}$ $\mathrm{km \cdot s^{-1}}$	$\log(L_{5100\AA})$ $\mathrm{erg \cdot s^{-1}}$	$\log(M_{BH})$ $M_\odot$	$\log(\dot{m})$
0	J000710.01+005329.0	0.3162	17.13	0.48	290.96±2.925	3414.60	44.09	8.78	−1.88
1	J032559.97+000800.7	0.3609	17.88		241.56±4.854	3868.92	44.62	8.45	−1.02
2	J075407.95+431610.5	0.3476	17.23	1.50	179.50±2.068	3718.52	44.68	7.94	−0.44
3	J113020.99+022211.4	0.2411	17.51	0.45u	325.12±4.467	3136.51	44.15	8.97	−2.01
4	J001224.02−102226.2	0.2282	16.91	0.65	270.19±8.137	3375.07	44.36	8.65	−1.48
5	J233254.46+151305.4	0.2147	17.23		193.32±2.888	3282.24	44.13	8.07	−1.12
6	J091828.59+513932.1	0.1854	17.13	0.43	149.72±2.815	2632.22	44.02	7.62	−0.79
7	J093653.84+533126.9	0.2280	16.86	0.53	266.58±3.254	2951.40	44.35	8.63	−1.46
8	J133957.99+613933.4	0.3724	18.68		309.30±9.214	3363.38	44.26	8.89	−1.81
9	J140019.27+631426.9	0.3314	17.76	0.55u	255.49±13.13	4611.71	44.44	8.55	−1.30
10	J154019.57−020505.4	0.3204	16.73	0.80	187.93±3.000	3953.81	44.83	8.02	−0.37
11	J2125−0813	0.6239	17.07	0.46	268.29±12.57	5026.95	45.21	8.64	−0.61
12	J084230.51+495802.3	0.3050	17.93	0.59u	239.02±6.430	2780.96	44.33	8.44	−1.29
13	J032225.40−081255.3	0.1260	17.96		141.04±3.522	2152.76	43.59	7.52	−1.11
14	J121018.35+015405.9	0.2158	17.23	0.30u	180.30±3.434	2617.29	44.33	7.94	−0.80
15	J222435.29−001103.8	0.0581	17.05		152.92±4.589	1975.48	43.26	7.66	−1.58
16	J103421.70+605318.1	0.2277	17.65	0.60u	127.02±6.491	2545.75	44.20	7.33	−0.31
17	J222055.73−075317.9	0.1489	17.60		188.47±7.977	2916.25	43.87	8.02	−1.33
18	J102914.87+572353.7	0.1885	17.79	0.53u	256.27±3.611	2312.89	43.99	8.56	−1.75
19	J094859.47+433518.9	0.2262	16.91	0.16u	150.49±2.132	2294.98	44.49	7.63	−0.32
20	J100756.46+491809.5	0.1496	17.98	0.60u	103.85±4.431	2252.58	43.73	6.98	−0.43
21	J095744.43+075124.8	0.1406	17.61	0.47u	134.84±5.772	2594.93	43.81	7.44	−0.81
22	J140502.65+470747.5	0.1521	17.54	0.42u	130.14±5.365	2782.77	43.92	7.37	−0.63
23	J151535.25+480530.5	0.3115	16.52	0.01u	192.45±6.467	2980.23	44.89	8.06	−0.35
24	J144207.69+384411.3	0.1457	17.48	0.40u	116.35±2.027	2643.79	43.91	7.18	−0.45
25	J153415.41+303435.4	0.0938	16.98	0.20u	183.73±2.272	2940.21	43.72	7.98	−1.44
26	J082930.59+081238.0	0.1291	17.21	0.32	165.72±1.981	3005.78	43.91	7.80	−1.07

Notes: The first Column lists the ID number of the object. The second and third Columns present the name in the format of "SDSS Jhhmmss.ss±ddmmss.s" and redshift of each object. The forth column presents the PSF magnitude in r band of SDSS. The fifth column gives the value of R_r (radio loudness) as defined by Ivezić et al. (2002), 'u' represents the value of an upper limit one. The following two columns list the line width of [NII]λ6583Å and broad Hα in units of $\mathrm{km \cdot s^{-1}}$. The last three columns contain the value of continuum luminosity at 5100 Å (corrected for Galactic extinction including the redden correction, following Schlegel et al. 1998), the value of BH masses estimated from the line width of [OIII]λ5007Å (as a tracer of velocity dispersion) and the dimensionless accretion rate of the dbp emitters.

The line width of broad Hα of J2125-0813 is estimated from the linewidth of broad Hβ produced by the accretion disk model. Here, we just list the PSF magnitude at r band for each object.

results indicate that the anti-correlation between EW(FeII)/EW(Hβ) and line width of broad lines is also valid for dbp emitters.

The correlation between FeII properties and the line width of Balmer broad lines reflects, to some extent, effects of the line of sight. In the case of the correlation between the FeII properties and the width of the narrow lines, which are considered as tracers of stellar velocity dispersion, the effect of the bulge-BH mass on the properties of FeII emission may be more neatly deconvolved. A detailed description about this is shown in the next subsection. Figure 5 shows the correlation between EW(FeII)/EW(Hβ) and line width of narrow lines. Here, we select the line width

TABLE 2

PARAMETERS OF THE ACCRETION DISK MODEL

Id	r_{in} R_g	r_{out} R_g	i	e	q	σ $km\cdot s^{-1}$	$k_{H\beta}$	k_{FeII}
0	991	4054	33	0.25	2.57	2032±754	0.39	0.35
1	391±62	4085±151	89±6	0.26±0.01	0.98±0.11	738±90	0.40	0.28
2	385	969	28	0.57	3.61	2059±400	0.43	0.13
3	367±37	11946±1077	50±3	0.24±0.01	1.71±0.01	296±25	0.37	0.11
4	37±17	2660±158	26±1	0.21±0.01	1.29±0.02	700±43	0.39	0.18
5	526±89	5557±833	54±5	0.21±0.01	1.29±0.08	771±60	0.47	0.21
6	526±21	3350±255	89	0.96±0.01	2.24±0.05	703±48	0.36	0.41
7	103±3	1804±29	21±0	0.27±0.02	1.21±0.01	915±21	0.36	0.10
8	2797	32768	89	0.17	7.40±1.86	1622±275	0.54	0.27
9	210±112	5705	47	0.03	1.43±0.20	1813±1078	0.34	0.42
10	394±40	4953±142	89	0.24±0.01	0.97±0.07	1238±55	0.34	0.35
11	31±6	339±40	15±1	0.01	1.58±0.19	2610±270	1.00	0.53
12	222±18	3382±374	85±2	0.90±0.01	2.03±0.04	624.6±46.5	0.45	0.44
13	30±8	12790±507	25±0	0.33±0.01	1.56±0.01	292±13	0.42	0.38
14	408±11	3100±116	86±1	0.94±0.01	2.15±0.02	562.5±40.5	0.51	0.42
15	578±340	32768	72	0.26±0.08	1.36±0.01	479±16	0.36	0.47
16	208±12	4830±333	85±2	0.84±0.01	1.85±0.02	499±24	0.44	0.36
17	11±1	7779±428	30±0	0.23±0.01	1.44±0.01	476.4±33.30	0.54	0.65
18	23±13	6843±387	23±0	0.34±0.01	1.54±0.03	461.4±27.00	0.53	0.40
19	88±7	3401±226	89±2	0.84±0.01	1.46±0.02	572.7±21.30	0.41	0.52
20	406±30	4875±346	84±7	0.87±0.01	1.92±0.04	451.5±32.40	0.51	0.53
21	141±43	26691±4774	54±7	0.28±0.01	1.50±0.01	429.6±23.70	0.30	0.23
22	99±19	15609±1578	44±2	0.32±0.01	1.63±0.01	303.9±23.70	0.51	0.75
23	104±16	13542±1252	41±2	0.33±0.01	1.73±0.01	461.7±27.30	0.54	0.42
24	99±13	2551±278	78±1	0.81±0.01	1.54±0.03	566.1±22.80	0.50	0.40
25	307±24	21499±1118	81±8	0.28±0.01	1.56±0.01	352.2±22.50	0.44	0.42
26	77±6	2285±150	76±8	0.83±0.01	1.71±0.02	676.8±29.10	0.39	0.36

Notes: If the error of the parameter is larger than the value of the parameter, we do not show the error. The id number represents the name in the Table 1.

of the [OIII] emission line. As described above, two Gaussian components are needed for [OIII] emission line: one normal (core) component and an extended one. We use the core components as described in Greene & Ho (2005a). The Spearman rank of the correlation coefficient is -0.52 with $P_{null} \sim 0.6\%$.

Moreover, we check the correlation between EW(FeII) and the ratio of the peak height of [OIII]λ5007Å to that of Hβ (peak λ5007Å) as described by Boroson & Green (1992). The correlation between EW(FeII) and peak λ5007Å discovered by Boroson & Green (1992) using a sample of low redshift quasars is confirmed for dbp emitters. The Spearman rank correlation coefficient is -0.24 with $P_{null} \sim 3\%$. The plot is shown in Figure 6. The result indicates that the parameter, peak λ5007Å, is a better indicator of dbp emitters with strong FeII emission lines.

Furthermore, we check the radio properties of dbp emitters with apparent FeII emission lines. We find that there are 8 dbp emitters in our sample targeted and 13 dbp emitters covered by FIRST/NVSS. Thus, we can get the radio flux density or the upper limit value of radio flux density at 20cm. According to the definition of radio loudness, R_i, by Ivezić et al. (2002):

$$R_i = log(F_{20cm}/F_i) = 0.4 \times (m_i - t) \qquad (2)$$

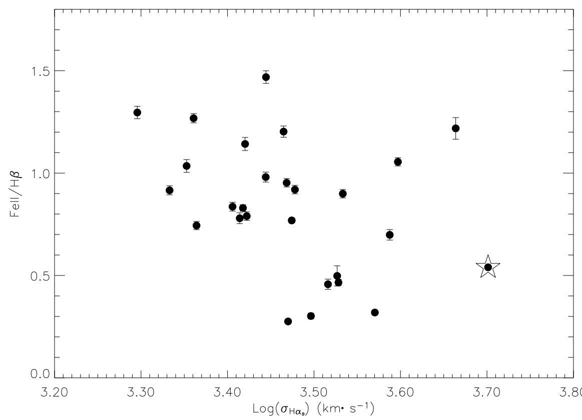

Fig. 4. The correlation between EW(FeII)/EW(Hβ) and the line width of broad Hα. The five-point star represents the object SDSS J2125-0813.

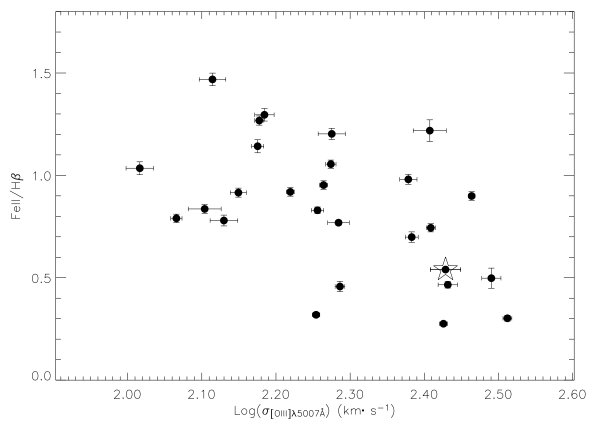

Fig. 5. The correlation between EW(FeII)/EW(Hβ) and the line width of [OIII]λ5007Å. The five-point star represents the object SDSS J2125-0813.

where m_i is one of the SDSS magnitudes and t is the 20cm AB radio magnitude defined as $t = -2.5\log(F_{20cm}/3631\text{Jy})$, we can calculate radio loudness for each dbp emitter in our sample. There is only one dbp emitter with $R_r > 1$, SDSS J075407.95+431610.5, which is a radio loud quasar. The other 20 dbp emitters are radio quiet quasars. Thus dbp emitters with stronger FeII emission lines are apt to be found in radio quiet quasars, which is in agreement with the E1 analysis of single peaked BRL AGN (e.g. Sulentic et al. 2003).

It is also convenient to check the correlation between the continuum luminosity and the luminosity of Hα, which is confirmed by Greene & Ho (2005b) using a sample of AGN selected from SDSS, because in our code the flux of Hα is one of fundamental parameters to determine the flux of other emission lines, such as the flux of double-peaked Hβ, $k_{H\beta} \times f_{H\alpha}$, the flux of FeII emission lines, and $K_{FeII} \times f_{H\alpha}$. One of the main considerations is that the correlation reflects some physical parameters of BLRs of AGN, such as the covering factor of BLRs, the proportional contribution of the ionization energy to the emission of broad emission lines, etc. The correlation is shown in Figure 7. The Spearman rank correlation coefficient is ~ 1 with $P_{null} \sim 0$. The correlation for dbp emitters obeys the same relation as that for normal AGN, $L_{H\alpha} \sim L^{1.157}_{5100\text{Å}}$. Here, the luminosity of Hα also includes the contributions of [NII] doublets, besides the contributions of broad and narrow components of Hα, because sometimes it is difficult to separate the narrow component of Hα from the components of [NII] for some dbp emitters. Because of the small contributions of [NII] emission lines, the relation between $L_{H\alpha}$ and $L_{5100\text{Å}}$ is not affected.

In the case of dbp we can get, from the best fitted results of the accretion disk model, the inclination angle of the accretion disk. The plot of the strength of FeII *vs.* the inclination angle of the accretion disk is shown in Figure 8. The Spearman Rank correlation coefficient is 0.43 with $P_{null} \sim 6\%$. We selected only 20 objects with accurate inclination angles i, $i > 1.5 \times i_{error}$. The inclination angle derived from the accretion disk model has a somewhat large error, specially when the angle is near 90 degrees. We cannot confirm a trend for all objects, because if we only consider the objects with inclination angle less than 60 degrees the coefficient is 0.16 with $P_{null} \sim 63\%$. On the other hand, if the trend between the strength of FeII emission lines and the inclination angle shown in Figure 7 were true, it would indicate that the objects with broader Balmer lines have stronger FeII emission lines, which is in contradiction with the much stronger correlation between strength of FeII emission lines and line width of broad Hα. It is also in contradiction with all previous results found from E1 parameter space analysis, e.g. Sulentic et al. (2000). Thus, the trend most be a fake one. This is due not only to the fact that values for the inclination have large errors for large angles, but also to the fact that inclination alone cannot govern the FeII strength, it is always convolved with BH mass and accretion rate, as discussed below (see also Marziani et al. 2003a)

3.3. *Influence of Black Hole Mass and Accretion Rate*

The most accurate way to estimate the central BH masses is by the stellar velocity dispersion as in

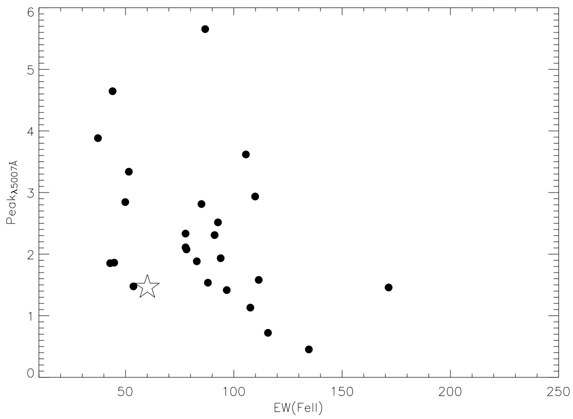

Fig. 6. The correlation between EW(FeII) and the height ratio of [OIII]λ5007Å to that of Hβ. The five-point star represents the object SDSS J2125-0813.

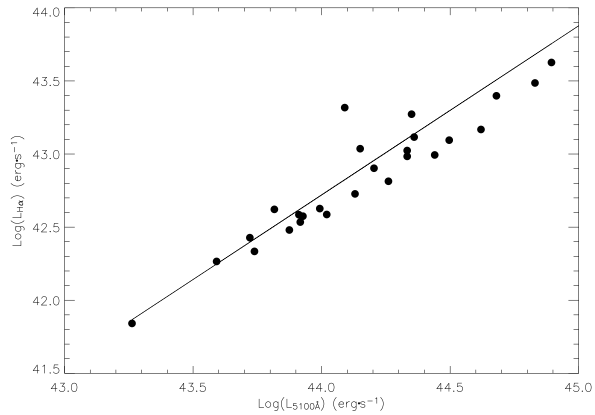

Fig. 7. The correlation between the continuum luminosity and the luminosity of Hα.

Gebhardt et al. (2000); Ferrarese & Merritt (2001); Tremaine et al. (2002). For quasars, it is not possible to determine the BH masses by the stellar velocity dispersion. Another convenient way is under the assumption of virialization (Greene & Ho 2005b; Ovcharov, Ivanov, & Nedialkov 2005; Wu et al. 2004; McLure & Jarvis 2004; 2002; Marziani, Dultzin-Hacyan, & Sulentic 2006; Onken et al. 2004; Peterson et al. 2004). However, there are various caveats for the measurement of the full width at half maximum (FHHM) of broad low-ionization emission lines, such Hβ, especially for dbp emitters. A detailed discussion of the line components that do reverberate can be found in Sulentic et al. (2006). Actually, these authors prefer to use the FeII lines (assuming they are virialized as we prove here to determine BH masses). Unfortunately, for double-peaked broad emission lines, it is not reasonable to fit the line by one Gaussian function or to measure the value of FWHM for double-peaked emission lines.

However, there is a strong correlation between stellar velocity dispersion and line width of low-ionization narrow emission lines, which has been studied by many authors for different kinds of AGN. Nelson & Whittle (1996) found that there is a correlation between line width of [OIII]λ5007Å and stellar velocity dispersion. Wang & Lu (2001) also emphasized the relation for a sample of NLS1s. Recently, Greene & Ho (2005a) confirmed that the line width of low-ionization narrow emission lines can trace the stellar velocity dispersion using a sample of low luminous AGN selected from SDSS (York et al. 2000; Strauss et al. 2002; Abazajian et al. 2004). Zhou et al. (2006) re-confirmed the stronger relation for a larger sample of NLSy1 selected from SDSS by line width of [NII] emission line. As a test, Boroson (2003) has shown the coincidence between the BH masses estimated from the relation $M_{BH} - \sigma_{[\mathrm{OIII}]}^{4.02}$ and the BH masses estimated under the assumption of virialization for a sample of AGN selected from SDSS.

As mentioned above, in order to determine the BH masses of the dbp emitters, we use the line width of [OIII] emission line as the estimator, according to the following equation (Gebhardt et al. 2000; Ferrarese & Merritt 2001; Tremaine et al. 2002):

$$M_{BH} = 10^{8.13\pm0.06}\left(\frac{\sigma_{[\mathrm{OIII}]}}{200\ \mathrm{km}\cdot\mathrm{s}^{-1}}\right)^{4.02\pm0.32} M_{\odot} \quad (3)$$

where $\sigma_{[\mathrm{OIII}]}$ is the line width of the normal component of [OIII]λ5007Å. The correlation between BH masses and EW(FeII)/EW(Hβ) has been pointed out above as the correlation between $\sigma_{[\mathrm{OIII}]\lambda5007Å}$ and EW(FeII)/EW(Hβ) (Figure 5) The anti-correlation of EW(FeII)/EW(Hβ) and line width of [OIII]λ5007Å indicates that the dbp emitters with lower BH masses have stronger FeII emissions. This result is in agreement with that of E1 analysis of single peaked BRL AGN (e.g. Sulentic et al. 2000).

The correlation between the dimensionless accretion rate and EW(FeII)/EW(Hβ) is shown in Figure 9. The dimensionless accretion rate $\dot{m}$ is calculated as $\dot{m} = 9 \times L_{5100Å}/M_{BH} \times 1.38 \times 10^{38}$ (Wandel, Peterson, & Malkan 1999; Kaspi et al. 2000). The Spearman rank correlation coefficient is 0.23 with $P_{null} \sim 24\%$. Such a weak correlation indicates that dimensionless accretion rate has weaker effects on FeII emission of dbp emitters than does the BH mass.

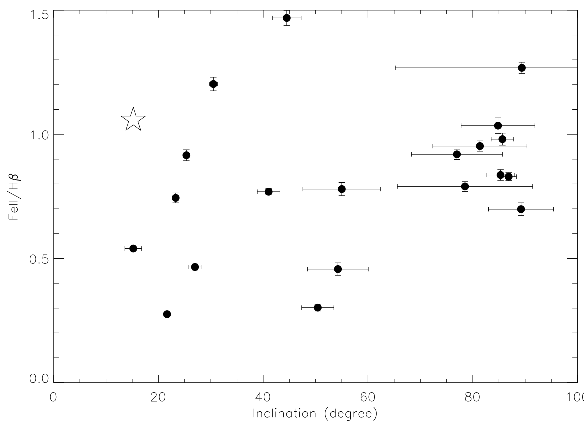

Fig. 8. The correlation between EW(FeII)/EW(Hβ) and the inclination angle of the accretion disk. The five-point star represents the object SDSS J2125-0813.

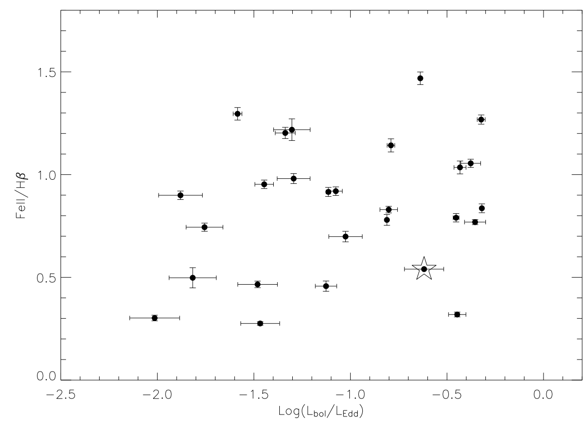

Fig. 9. The correlation between accretion rate and EW(FeII)/EW(Hβ). The five-point star represents the object SDSS J2125-0813.

The mean BH masses for the 27 dbp emitters is $10^{8.05\pm0.11}$ $M_{\odot}$, the mean dimensionless accretion rate is $10^{-1.04\pm0.11}$. According to the dimensionless accretion rate, the accretion mode in the central region is standard accretion rather than ADAF mode, because the upper limit accretion rate for ADAF mode is about $\dot{m} \sim 0.28 \times \alpha^2$ where α is viscous coefficient $\alpha \sim 0.1 - 0.3$ (Mahadevan & Quataert, 1997; Lasota et al. 1996; Narayan, Yi, & Mahadevan 1995). If we select $\alpha \sim 0.1$ (Yi, 1996; Choi, Yang, & Yi 2001), all the dbp emitters in our sample have larger accretion rates than the critical value 0.0028. Furthermore, the 27 dbp emitters have normal quasar spectra, with normal big blue bumps. Thus, even if ADAF accretion mode dominates the accretion flow in the inner region of the accretion disk, especially for the two objects with lower accretion rate, the standard accretion mode should mainly dominate the bulk of accretion.

4. DISCUSSIONS AND CONCLUSIONS

We have accurately reproduced the line profiles in the wavelength range from 4100 Å to 5600 Å by the line profile of double-peaked broad Hα. The best fitted results indicate that the broad optical FeII emission lines are also double-peaked and originate from the same place where the double-peaked broad Balmer emission lines. More and more evidence confirms that the double-peaked broad low-ionization lines come from the accretion disk rather than from an outflow or other models. In our sample, the double-peaked broad Hα of all the 27 dbp emitters can be best fitted by the elliptical accretion disk model (Eracleous et al. 1995). The best fitted results for the optical FeII emission lines indicate that the FeII emission lines also originate from the accretion disk which provides the needed high density for these lines.

The accretion rate and the normal quasar spectra indicate that ADAF accretion mode in the dbp emitters with FeII emission lines is not the main accretion mode. BH masses have more influence on the FeII properties of dbp emitters than the dimensionless accretion rate. The reliable anti-correlation between EW(FeII)/EW(Hβ) and $\sigma_{H\alpha}$ indicates that for dbp emitters the emission region of stronger FeII lines are far from the central black hole. We have shown that even for dbp emitters the influence of orientation on FeII intensity cannot be deconvolved from the other determining physical parameters of these AGN: mainly BH mass and, to a lesser extent, accretion rate.

We also obtain the same strong correlation between $L_{5100\text{Å}}$ and $L_{H\alpha}$ (including the broad and narrow components near Hα) for dbp emitters in our ample as that obeyed by normal AGN, which indicates that the connection between the continuum and BLRs is the same for normal AGN and for dbp emitters. We know that the luminosity of broad emission lines, such as broad Hα, can be estimated as $L_{H\alpha} = h\nu_{H\alpha} n_e n_H \alpha_{H\alpha} \epsilon V$, where $\alpha_{H\alpha}$ is the recombination coefficient for Hα, and ϵV is the volume filled by gas in BLRs. The electron density in the accretion disk is larger than that in the normal BLRs, which indicates that the value of $n_e n_H \alpha_{H\alpha} \epsilon V$ is a constant for AGN, normal AGN and dbp emitters

Finally we want to stress that the correlations, or more precisely perhaps, the trends pointed out above remain to be confirmed, because of two main reasons: first, the comparative numbers of well defined dbp emitters is small (which is intriguing enough), and second, because one of our selection criteria (the apparent strehgth of optical FeII) may bias the trends.

ZXG gratefully acknowledges the postdoctoral scholarships offered by Universidad Nacional Autónoma de México (UNAM). D. D-H acknowledges support from grant IN100703 from DGAPA, UNAM. This research has made use of the NASA/IPAC Extragalactic Database (NED) which is operated by the Jet Propulsion Laboratory, California Institute of Technology, under contract with the National Aeronautics and Space Administration. This paper has also made use of the data from the SDSS projects. Funding for the creation and the distribution of the SDSS Archive has been provided by the Alfred P. Sloan Foundation, the Participating Institutions, the National Aeronautics and Space Administration, the National Science Foundation, the U.S. Department of Energy, the Japanese Monbukagakusho, and the Max Planck Society. The SDSS is managed by the Astrophysical Research Consortium (ARC) for the Participating Institutions. The Participating Institutions are The University of Chicago, Fermilab, Institute for Advanced Study, Japan Participation Group, The Johns Hopkins University, Los Alamos National Laboratory, Max-Planck-Institute for Astronomy (MPIA), Max-Planck-Institute for Astrophysics (MPA), New Mexico State University, Princeton University, United States Naval Observatory, and University of Washington.

REFERENCES

Abazajian, K., et al. 2004, AJ, 128, 502
Antonucci, R., Hurt, T., & Agol, E. 1996, ApJ, 456, 25
Baldwin, J. A., Ferland, G. F., Korista, K. T., Hamann, A., & LaCluyze, A. 2004, ApJ, 615, 610
Baldwin, J. A., Ferland, G. F., Korista, K. T., & Verner, D. 1995, ApJ, 455, L119
Begelman, M. C., Blandford, R. D., & Rees, M. J. 1980, Nature, 287, 307
Bergeron, J., & Knuth, D. 1980, A&A, 85, L11
Boroson, T. A. 2003, ApJ, 584, 647
Boroson, T., A., & Green, R. F. 1992, ApJS, 80, 109
Bottorff, M., Ferland, G., Baldwin, J., & Korista, K. 2000, ApJ, 542, 644
Chen, K. Y., & Halpern, J. P. 1989a, ApJ, 344, 115
Chen, K. Y., Halpern, J. P., & Filippenko, A. V. 1989b, ApJ, 339, 742
Chen, K. Y., Halpern, J. P., & Titarchuk, L. G. 1997, ApJ, 483, 194
Choi, Y.-Y., Yang, J., & Yi, I. 2001, ApJ, 555, 673
Collin-Souffrin, S., Hameury, J. M., & Joly, M. 1988, A&A, 205, 19
Collin-Souffrin, S., Joly, M., Péquignot, D., & Dumont, S. 1986, A&A, 166, 27
Dumont, A. M., Collin-Souffrin, S., & Nazarova, L. 1998, A&A, 331, 11
Eracleous, M., & Halpern, J. P. 1994, ApJS, 90, 1
_________. 2003, ApJ, 599, 886
Eracleous, M., Halpern, J. P., Gilbert, A. M., Newman, J. A., & Filippenko, A. V. 1997, ApJ, 490, 216
Eracleous, M., Livio, M., Halpern, J. P., & Storchi-Bergmann, T. 1995, ApJ, 438, 610
Ferland, G. J., & Person, S. E. 1989, ApJ, 347, 656
Ferrarese, L., & Merritt, D. 2001, MNRAS, 320, L30
Francis, P. J., Hewett, P. C., Foltz, C. B., Chaffee, F. H., Weynmann, R. J., & Morris, S. L. 1991, ApJ, 373, 465
Gaskell, C. M. 1983, Nature, 304, 212
Gebhardt, K., et al. 2000, ApJ, 439, L13
Gilbert, A. M., Eracleous, M., Filippenko, A. V., & Halpern J. P. 1999, BAAS, 31, 950
Grandi, S. A. 1981, ApJ, 251, 451
_________. 1982, ApJ, 255, 25
Greene, J. E., & Ho, L. C. 2005a, ApJ, 627, 721
_________. 2005b, ApJ, 630, 12
Halpern, J. P., Eracleous, M., Filippenko, A. V., & Chen, K. Y. 1996, ApJ, 464, 704
Hao, L., et al. 2005, AJ, 129, 1783
Hartnoll, S. A., & Blackman, E. G. 2002, MNRAS, 332, L1
Ivezić, Z., et al. 2002, AJ, 124, 2364
Joly, M. 1987, A&A, 184, 33
_________. 1991, A&A, 242, 49
Karas, V., Martocchia, A., & Subr, L. 2001, PASJ, 53, 189
Kaspi, S., Smith, P. S., Netzer, H., Maoz, D., Jannuzi, B., & Giveon, U. 2000, ApJ, 533, 631
Korista, K., Baldwin, J., Ferland, G., & Verner, D. 1997, ApJS, 108, 40
Kwan, J., Cheng, F.-Z., Fang, L.-Z., Zheng, W., & Ge, J. 1995, ApJ, 440, 628
Laor, A., Jannuzi, B. T., Green, R. F., & Boroson, T. A. 1997, ApJ, 489, 656
Lasota, J. P., Abramowicz, M. A., Chen, X., Krolik, J., Narayan, R., & Yi, I. 1996, ApJ, 462, 142L
Li, C., Wang, T. G., Zhou, H. Y., Dong, X. B., & Cheng, F. Z. 2005, AJ, 129, 669
Mahadevan, R., & Quataert, E. 1997, ApJ, 490, 605
Marziani, P., Dultzin-Hacyan, D., & Sulentic, J. W. 2006, New Developments in Black Hole Research (New York: Nova Science Publisher Inc.)
Marziani, P., Sulentic, J. W., Zamanov, R., Calvani, M., Dultzin-Hacyan, D., Bachev, R., & Zwitter, T. 2003a, ApJS, 145, 199
Marziani, P., Zamanov, R., Sulentic, J. W., Dultzin-Hacyan, D., Bongardo, C., & Calvani, M. 2003b, in ASP Conf. Ser. 290, Active Galactic Nuclei: From Center Engine to Host Galaxy, ed. S. Collin,

F. Combes, & I. Shlosman (San Francisco: ASP), 229
McLure, R. J., & Jarvis, M. J. 2002, MNRAS, 337, 109
_________. 2004, MNRAS, 353, 45
Moore, C. E., & Merill, P. W. 1968, in NSRDS-NBS 23, Partial Grotrian Diagrams of Astrophysical Interest (Washington: US Government Printing Office)
Narayan, R., Yi, I., & Mahadevan, R. 1995, Nature, 374, 623
Nelson, C. H., & Whittle, M. 1996, ApJ, 465, 96
Netzer, H. 1985, ApJ, 289, 451
_________. 1988, in IAU Colloq. 94, Physics of Formation of FeII Lines outside LTE, ed. R. Viotti, A. Vittone, & M. Friedjung (Dordrecht: Reidel), 247
Oke, J. B., & Lauer, T. R. 1979, ApJ, 230, 360
Onken, C. A., Ferrarese, L., Merritt, D., Peterson, B. M., Pogge, R. W., Vestergaard, M., & Wandel, A. 2004, ApJ, 615, 645
Ovcharov, E., Ivanov, V. D., & Nedialkov, P. 2005, in Growing Black Holes: Accretion in a Cosmological Context, ESO Astrophysics Symposia, ed. A. Merloni, S. Nayakshin, & R. A. Sunyaev (Berlin: Springer), 134
Penston, M. V. 1988, MNRAS, 233, 601
Peterson, B. M., et al. 2004, ApJ, 613, 682
Phillips, M. M. 1978, ApJ, 226, 736
_________. 1979, ApJS, 39, 377
Schlegel, D., Finkbeiner, D. P., & Davis, M. 1998, ApJ, 500, 525
Shapovalova, A. I., et al. 2001, A&A, 376, 775
Sigut, T. A., & Pradhan, A. K. 1998, ApJ, 499, L139
_________. 2003, ApJS, 145, 15
Storchi-Bergmann, T., Baldwin, J. A., & Wilson, A. S. 1993, ApJ, 410, L11
Storchi-Bergmann, T., Eracleous, M., Livio, M., Wilson, A., Filippenko, A., & Halpern, J. 1995, ApJ, 443, 617
Storchi-Bergmann, T., Eracleous, M., Ruiz, M., Livio, M., Wilson, A., & Filippenko, A. 1997, ApJ, 489, 87
Storchi-Bergmann, T., et al. 2003, ApJ, 598, 956
Strateva, I. V., et al. 2003, AJ, 126, 1720
Strauss, M., et al. 2002, AJ, 124, 1810
Sulentic, J. W., Marziani, P., & Dultzin-Hacyan, D. 2000, ARA&A, 38, 521
Sulentic, J. W., Repetto, P., Stirpe, G. M., Marziani, P., Dultzin-Hacyan, D., & Calvani, M. 2006, A&A, 456, 926
Sulentic, J. W., Zamfi, S., Marziani, P., Bachev, R., Calvani, M., & Dultzin-Hacyan, D. 2003, ApJ, 597, L17
Sulentic, J. W., Zheng, W., Calvani, M., & Marziani, P. 1990, ApJ, 355, 15
Tremaine, S., et al. 2002, ApJ, 574, 740
Vanden Berk, D. E., et al. 2001, AJ, 122, 549
Verner, E. M., Verner, D. A., Korista, K. T., Ferguson, J. W., Hamann, F., & Ferland, G. J. 1999, ApJS, 120, 101
Wandel, A., Peterson, B. M., & Malkan, M. A. 1999, ApJ, 526, 579
Wang, T. G., & Lu, Y. J. 2001, A&A, 377, 52
Wills, B. J., Netzer, H., Uomoto, A. K., & Wills, D. 1980, ApJ, 237, 319
Wills, B. J., Netzer, H., & Wills, D. 1980, ApJ, 241, L1
Wu, X. B., Wang, R., Kong, M. Z., Liu, F. K., & Han, J. L. 2004, A&A, 424, 793
Yi, I. 1996, ApJ, 473, 645
York, D. G., et al. 2000, AJ, 120, 1579
Zhang, X.-G., Dultzin-Hacyan, D., & Wang, T.-G. 2006a, MNRAS, 372, L5 (Paper I)
_________. 2007, in preparation
Zheng, W., Kriss, G. A., Telfer, R. C., Grimes, J. P., & Davidsen, A. F. 1997, ApJ, 475, 469
Zheng, W., Sulentic, J. W., & Binette, L. 1990, ApJ, 365, 115
Zhou, H.-Y., Wang, T.-G., Yuan, W., Lu, H., Dong, X., Wang, J., & Lu, Y. 2006, ApJS, 166, 128

Deborah Dultzin-Hacyan and Xue-Guang Zhang: Instituto de Astronomía, Universidad Nacional Autónoma de México, Apdo. Postal 70-264, México D. F. 04510, Mexico (deborah, xguang@astroscu.unam.mx).
Ting-Gui Wang: Center for Astrophysics, Department of Astronomy and Applied Physics, University of Science and Technology of China, Hefei, Anhui, P.R. China (twang@ustc.edu.cn).